TÜBİTAK

Turkish Journal of Chemistry

http://journals.tubitak.gov.tr/chem/

Research Article

Turk J Chem
(2023) 47: 280-293

doi:10.55730/1300-0527.3536

Promoting antihepatocellular carcinoma activity against human HepG2 cells via pyridine substituted palladium complexes: in vitro evaluation and QSAR studies

Öğünç MERAL[1], Fatih Mehmet EMEN[2,*], Emine KUTLU[2], Ruken Esra DEMİRDÖĞEN[3], Neslihan KAYA KINAYTÜRK[4], Görkem KISMALI[1], Şevkinaz DOĞAN[5]

[1]Department of Biochemistry, Faculty of Veterinary Medicine, Ankara University, Ankara, Turkey
[2]Department of Chemistry, Faculty of Arts and Sciences, Burdur Mehmet Akif Ersoy University, Burdur, Turkey
[3]Department of Chemistry, Faculty of Science, Çankırı Karatekin University, Çankırı, Turkey
[4]Department of Nanoscience and Nanotechnology, Faculty of Arts and Sciences, Burdur Mehmet Akif Ersoy University, Burdur, Turkey
[5]Department of Nursing, Faculty of Health Sciences, Burdur Mehmet Akif Ersoy University, Burdur, Turkey

Received: 12.08.2022 • **Accepted/Published Online:** 04.01.2023 • **Final Version:** 20.02.2023

Abstract: Bis(4-(4-nitrobenzyl)pyridine)dichloropalladium(II), $[PdCl_2L^1_2]$, bis(2-amino-5-bromopyridine)dichloropalladium(II), $[PdCl_2L^2_2]$, bis(2,4-dimethylpyridine)dichloropalladium(II), $[PdCl_2L^3_2]$, bis(3,4-dimethylpyridine)dichloropalladium(II), $[PdCl_2L^4_2]$ were prepared. The spectroscopic techniques (FT-IR and ^{1}H-NMR, ^{13}C-NMR) were used to characterize the compounds. Theoretical calculations were used to validate the experimental results. The LanL2DZ-based DFT/B3LYP method was used to define the most stable possible molecular structure for the complexes. Potential energy distribution analysis was performed to determine the theoretical vibration bands of the complexes. Molecular electrostatic potential maps, boundary molecular orbitals and Mulliken charge distribution were used to determine the active sites of the molecules. The interaction mechanisms between the complexes and liver cancer protein were investigated via molecular docking. The study on the antiproliferative effects of these complexes on hepatocellular carcinoma cells (HepG2) showed that they are potent candidates for use against this liver cancer cell line.

Key words: Pyridine-palladium complexes, hepatocellular carcinoma, cell death, liver cancer

1. Introduction

Cancer, which is a complex disease characterized by uncontrolled cell proliferation, is the second largest cause of mortality in the world [1, 2]. Among other cancer types hepatocellular carcinoma (HCC), which is the most common type of primary liver cancer in adults, was the third most common cause of cancer deaths in 2020 in the world [3]. The highest incidence and the lowest survival rate after treatment for HCC was observed in Asia and sub-Saharan Africa where hepatitis B infection is endemic [4]. It is foreseen that new cancer cases will increase significantly in the next decades [4–7]. There are many types of cancer treatment options which are usually very complex and they are developing gradually. Among them are chemotherapy, surgery, and radiation therapy. Chemotherapy entails use of special drugs to kill cancer cells and has been recently supported by new methods of treatment such as immunotherapy to give successful results. However, chemotherapeutics have many negative side effects which compromises effectiveness of this treatment method. Therefore, recently increasing importance and efforts are devoted to development of more effective chemotherapeutic drugs with fewer side effects [8,9].

Metal-based compounds have attracted much attention since *cis*-platin was discovered by Barnett Rosenberg in 1960 and they have been used widely in treatment of various cancer types, especially of head and neck, ovarian and colorectal cancers. Today, *cis*-platin and its derivatives (i.e. carboplatin and oxaliplatin) are still extensively used in cancer treatment [10]. However, these compounds have major disadvantages such as the limitation of their efficacy to some cancer types as well as their extensive side effects [11]. Hence, recently new studies on other metal complexes have increased. Among these metal complexes, cost effective palladium complexes have attracted much attention as they form compounds similar to platinum [12]. Studies revealed that palladium (II) complexes have considerable anticancer activity on various cancer cell lines [13]. The many different types of Pd (II) complexes (i.e. monomeric, dimeric, tetrameric, cyclo-palladated, palladacyclic, and heterobimetallic) were reported to have cytotoxic activity and the pyridine, pyrazole, quinoline and,

* Correspondence: femen@mehmetakif.edu.tr

1,10-phenanthroline derivates of Pd (II) have great antiproliferative activity and all of them are promising anticancer agents as these complexes are more soluble than platinum complexes [14]. Despite the large number of reports on pyridine derivative complexes (i.e. chloropyridine, bromopyridine [15], methylpyridine [16], (p-tolyl) pyridine [17], (2,4 dinitrobenzyl) and ((2,4,6 trinitrobenzyl) pyridine) [18] only a very few of them are related to their anticancer effect. Studies showed that these pyridine derivatives can be exploited as anticancer drugs [19] with the effective mechanism of action of Pd complexes that proceeds over inhibition of cell proliferation of cancer cells via DNA binding [14]. Tabrizi et al. reported that the palladium complexes (II) with 2,2′-bipyridine (bpy) ligands have remarkable cytotoxic activity against the colorectal adenocarcinoma (HT-29), the breast (MCF-7), and the human squamous cervical adenocarcinoma (HeLa) cancer cell lines which was better than the effect of cisplatin [20]. In a study by Kuduk-Jaworska et al., palladium(II) complexes with 2,6-dimethyl-4-nitropyridine complexes were observed to have strong antiproliferative effect against adenocarcinoma of the rectum (SW707), breast cancer (T47D), bladder cancer (HCV) and nonsmall cell lung carcinoma (A549) cancer cell lines [21]. Franich et al. investigated the antiproliferative activity of palladium(II) with 4,4′-bipyridine ligands on murine lung cancer (LLC1 cells) and they reported that they had similar cytotoxic effect to cisplatin [22].

In this study, bis(4-(4-nitrobenzyl)pyridine)dichloropalladium(II), [$PdCl_2L^1_2$], bis(2-amino-5-bromopyridine) dichloropalladium(II), [$PdCl_2L^2_2$], bis(2,4-dimethylpyridine)dichloropalladium(II), [$PdCl_2L^3_2$], bis(3,4-dimethylpyridine) dichloropalladium(II), [$PdCl_2L^4_2$] were synthesized and characterized via spectroscopic techniques (FT-IR and ^{1}H-NMR, ^{13}C-NMR). The antiproliferative effects of these complexes on hepatocellular carcinoma cells (HepG2) were investigated and the interaction mechanisms of liver cancer protein and complexes were investigated by molecular docking studies.

2. Experimental

2.1. Materials

All chemicals and solvents used were of high purity and were used without further purification. $PdCl_2$ was supplied from Sigma Aldrich and 4-(4-nitrobenzyl)pyridine, 2-amino-5-bromopyridine, 2,4-dimethylpyridine, 3,4-dimethylpyridine and ethanol were supplied from Merck.

2.2. Synthesis of the complexes

The complexes were synthesized by reacting $PdCl_2$ with the pyridine derivatives in ethanol (Scheme). A solution of $PdCl_2$ (1.2 mol) was prepared in 50 mL of distilled water. The ethanolic solutions of the ligands (30 mL) were prepared by dissolving 2.4 mol of the ligands (L^1:4-(4-nitrobenzyl)pyridine, L^2:2-amino-5-bromopyridine,L^3:2,4-dimethylpyridine,L^4:3,4-dimethylpyridine). These solutions were added to the palladium solution under constant stirring and reflux for 2 h. Then thus obtained precipitates were filtered and dried.

Bis(4-(4-nitrobenzyl)pyridine)dichloropalladium(II), [$PdCl_2L^1_2$] : FT-IR (KBr, ν_{max}, cm^{-1}): 3080 ν(Ar-C–H), 2925–2854 ν(Al-C–H), 1614–1537 ν(Ar-C = C, C = N), 1350 ν(N–O), 1110–1016 δ(C–H in-plane), 880–518 δ(C–C in-plane), 470 ν(Pd–N). ^{1}H-NMR (d6-DMSO, ppm): 8.64–7.42 (16 H, Ar-H), 4.24 (4 H, Al-H). ^{13}C-NMR (d6-DMSO, ppm): 152.5 (4 C, o-Ar-C), 149.4 (p-Ar-C),146.0 (C-NO_2), 146.2 (Ar-C), 130.1 (Ar-C), 125.3 (m-Ar-C), 123.6 (Ar-C), 40.0 (CH_2). TOF-MS (ESI$^+$) for $C_{24}H_{20}Cl_2N_4O_4Pd$ (Acetonitrile), [M+7 H]$^+$, *m/z*: calcd. 612.8246 found 612.077.

Bis(2-amino-5-bromopyridine)dichloropalladium(II), [$PdCl_2L^2_2$] : FT-IR (KBr, ν_{max},cm^{-1}): 3427–3180 ν(N–H), 3076 ν(Ar-C–H), 2985–2839 ν(Al-C–H), 1622–1402 ν(Ar-C = C, C = N), 1265–1145 δ(C–H in-plane), 889 ν(C–Br), 823–503 δ(C–C in-plane), 476 ν(Pd–N). ^{1}H-NMR (d6-DMSO, ppm): 8.76–6.14 (6 H, Ar-H), 7.64 (4 H, N-H). ^{13}C-NMR (d6-DMSO, ppm): 158.1 (C -NH_2), 149.3 (o-Ar-C), 140.5 (p-Ar-C), 112.3 (m-Ar-C), 103.5 (C-Br).

Bis(2,4-dimethylpyridine)dichloropalladium(II), [$PdCl_2L^3_2$]: FT-IR (KBr,ν_{max},cm^{-1}): 3030 ν(Ar-C–H), 2950–2886 ν(Al-C–H), 1600–1473 ν(Ar-C = C, C = N),1251–1043 δ(C–H in-plane), 885–657 δ(C–C in-plane), 503 ν(Pd–N). ^{1}H-NMR (d6-DMSO, ppm): 8.40–7.65 (6H, Ar-H), 3.31-2.26 (12H, Al-H). ^{13}C-NMR (d6-DMSO, ppm): 150.2 (o-Ar-C), 140.6 (p-Ar-C), 134.9 (m-Ar-C), 17.9 (-CH_3). TOF-MS (ESI$^+$) for $C_{14}H_{18}Cl_2N_4O_4Pd$ (Dichloromethane), [M+6 H]$^+$, *m/z*: calcd. 397.6774 found 398.0350.

Bis(3,4-dimethylpyridine)dichloropalladium(II), [$PdCl_2L^4_2$] : FT-IR (KBr, ν_{max},cm^{-1}): 3035 ν(Ar-C–H), 2990–2806 ν(Al-C–H), 1612–1415 ν(Ar-C = C, C = N),1250–1089 δ(C–H in-plane), 856–524 δ(C–C in-plane), 433 ν(Pd–N).^{1}H-NMR (d6-DMSO, ppm): 8.45–7.30 (6H, Ar-H), 3.31–2.24 (12H, Al-H). ^{13}C-NMR (d6-DMSO, ppm): 151.5 (o-Ar-C), 149.9 (p-Ar-C), 134.2 (m-Ar-C), 18.5 (-CH_3).

2.3. Instrumentation

FTIR spectra (4000 to 400 cm^{-1}) were recorded using the Perkin Elmer Frontier FTIR spectrometer. Samples were taken in KBr pellets. NMR spectra were recorded using the Bruker Ultrashield Plus Biospin Avance III 400 MHz NanoBay FT-NMR instrument. d6-DMSO was used as solvent. Full mass analysis was performed by scanning in the positive (ES+) 50 – 1000 Da range via High Resolution Mass Spectrometry using Waters SYNAPT G1 MS system.

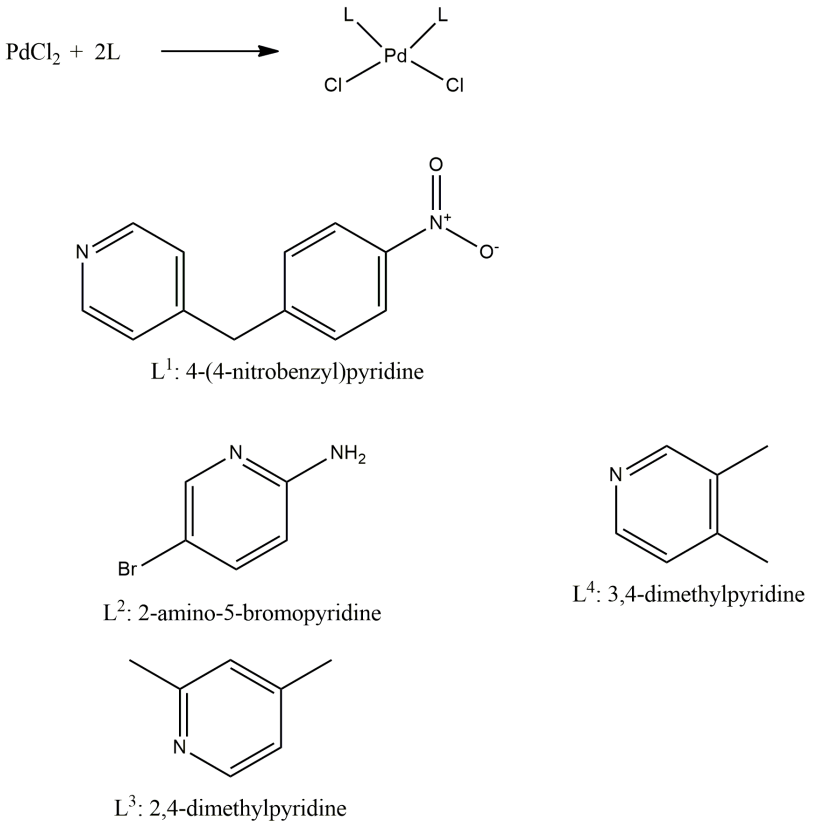

Scheme. Synthesis reaction of the complexes.

2.4. Cell culture studies

The HepG2 cell line was obtained from ATCC (Wesel, Germany, Cat. HB-8065) and maintained in RPMI-1640 medium with L-Glutamine (584 mg L^{-1}) (Irvine Scientific, Santa Ana, CA, USA) containing 10% (w/v) FBS (Irvine Scientific, Santa Ana, CA, USA) and gentamicin sulfate solution (50 µg mL^{-1}) (Irvine Scientific, Santa Ana, CA, USA). Seventy-five square centimeters cell culture flasks (BD Falcon, Rockville, MD, USA) were used to grow the cells and the process was carried out in a humidified (5% CO2) incubator at 37 °C. The culture medium was changed every two days. Cells were subcultured with trypsin-EDTA solution (1:4, v/v) (Irvine Scientific, Santa Ana, California, USA).

2.5. Cell proliferation/viability assay

One hundred microliters of culture medium, 96-well flat-bottom cell culture plates (Greiner Bio One, Frickenhausen, Germany) at a density of 1 × 105 cells/well were used for seeding HepG2 cells. After 24 h of incubation, both unbound and dead cells were removed by washing twice with buffer solution (PBS, Irvine Scientific, Santa Ana, California, USA) prior to all assays. The cytotoxic effect of the complexes was determined by measuring mitochondrial dehydrogenase activity in HepG2 cells using methyl thiazolyl tetrazolium (MTT) as substrate. Different concentrations of the complexes were dissolved in RPMI-1640 medium (3.12, 6.25, 12.5, 25, 50, 100, and 200 µM) and were added to the cells which were then treated for 24 h. After incubation, cells were washed with fresh medium. One hundred microliters of MTT (5 mg mL^{-1}) solution was added to all control and experimental cell groups. After 4 h of incubation, sodium dodecyl sulfate solution (10% (w/v), 100 µL) was added to each well to dissolve the formazan salt. The amount of formazan salts was quantified by measuring the absorbance value sat 570 nm in a microtiter plate reader (Sunrise, Tecan GmbH, Austria). IC50 values were calculated according to the MTT Assay results. Cell viability analysis was performed via one-way ANOVA followed by unpaired Student t-test. The IC50 values were calculated according to nonlinear quadratic model. p values <0.05 were considered to be statistically significant. Each experiment was performed in triplicates.

2.6. Evaluation of cell injury

Cell damage was assessed by measuring the release of lactate dehydrogenase (LDH) from the cells to the bath medium consisting of LDH. Cells were taken into 96-well plates and were incubated for 24 h after adding the complexes at different

concentrations (3.12, 6.25, 12.5, 25, 50, 100, and 200 μmol L^{-1}). LDH concentration in the Supernatant was determined by using Clinical Chemistry Analyzer (ERBA XL 600, Meinheim, Germany) and a commercial colorimetric assay kit (TML Medical, Ankara, Turkey). Total LDH release, which caused HepG2 cell death, was determined. Each experiment was performed in triplicates.

2.7. Computational details

Theoretical calculations were performed using Gaussian 09 software [23]. Quantum chemical calculations were performed using the B3LYP functional and LanL2DZ basis set and the density functional theory (DFT) method. B3LYP vibrational wave-numbers were found to be higher than experimental wave-numbers. Therefore, the scaling factor was used for the wave numbers and the mismatch effects were not taken into consideration. The wave-numbers calculated by B3LYP/Lanl2DZ bases set were scaled in the infrared spectra by 0.96, 1, 0.98, and 0.85 in the ranges [4000–2001] cm^{-1}, [2000–1407] cm^{-1}, [1406–341] cm^{-1} and [340–0] cm^{-1}, respectively [24]. In general, the scaled wave-numbers were calculated and were found to be in good agreement with the experimental ones. The geometry was optimized after performing the frequency calculations by using the same basis set. The results were visualized by using Gauss View software [25]. Total energy distribution was calculated using VEDA software [26]. The 3D crystal structure of the targeted protein (PDB ID: 2OH4) was obtained using the RSBC PDB format. The optimized structures of the complexes were determined using the DFT/B3LYP/LanL2DZ basis set. Molecular docking studies were performed using Hex (version 8.0.0) software [27]. In molecular docking studies FFT mode: 3D fast lifetime; distance range: 40; twist range: 360; correlation type: shape + electro + DARS; grid size: 0.6; receptor spacing: 180 and ligand spacing: 180 parameters were used. PyMOL molecular graphics software was used to visualize the data obtained from the HEX 8.00 software [28].

3. Results and discussion

3.1. Synthesis of the complexes

The complexes were synthesized according to the method given elsewhere [19]. The pyridine derivatives were reacted with the palladium chloride solution prepared in ethanol by refluxing. The formation of these complexes is pH-dependent and there were obtained in the pH range 2–3. Therefore, the pH of the media was adjusted to 2–3 via ammonia and the brown colored complexes were separated after precipitating. After washing with ethanol a few times they were dried in the oven at 70 °C. In our previous work [19] the complexes were not further purified since they could have been precipitated in the pure form.

3.2. Structural analysis of the complexes

The FT-IR spectra of the complexes were obtained in the range 4000–400 cm^{-1}. The experimental FT-IR data of the complexes are presented in Table 1 and the vibrational bands conferred to them are presented in Table S1 (in supporting information) in detail.

For all the complexes, while the vibrational band observed at 3030–3080 cm^{-1} indicates the Ar-H streching in the pyridine (Py) ring, the weak bands observed at 2990–2806 cm^{-1} indicates the C-H stretching vibrations of the aliphatic C-H groups. The intense bands observed in the range 1622–1402 cm^{-1} belong to the aromatic C=C and C=N stretching vibrations in the pyridine (Py) ring. The bands observed in the range 1265–1016 cm^{-1} show the in-plane C-H bending vibrations. The bands observed in the range 880–503 cm^{-1} indicate the C-C bending vibrations (in-plane). The vibrational band at 503–433 cm^{-1} indicates the Pd-N stretching vibrations. Beside the common stretching vibrations of the synthesized complexes the intense peaks observed with the $[PdCl_2L^1{}_2]$ complex at 1350 cm^{-1} indicate the N-O stretching vibrations of the nitro group. For the $[PdCl_2L^2{}_2]$ complex, the intense bands observed in the range 3427–3180 cm^{-1} indicate the N-H stretching vibrations of the NH_2 group bound to the Py ring at the ortho position. The weak bands observed at 889 cm^{-1} indicate the C-Br stretching vibrations. These experimental findings were supported with the theoretical calculations. The

Table 1. The selected stretching and bending vibrations of the complexes.

Complex	(N-H) cm^{-1}	(Ar-H) cm^{-1}	(Al-H) cm^{-1}	(C=C, C=N) cm^{-1}	(C-H) in-plane, cm^{-1}	(C-C) in-plane, cm^{-1}	(C-Br) cm^{-1}	(Pd-N) cm^{-1}
$[PdCl_2L^1{}_2]$	-	3080	2925–2854	1614–1537	1110–1016	880–518	-	470
$[PdCl_2L^2{}_2]$	3427	3076	2985–2839	1622–1402	1265–1145	823–503	889	476
$[PdCl_2L^3{}_2]$	-	3030	2950–2886	1600–1473	1251–1043	885–657	-	503
$[PdCl_2L^4{}_2]$	-	3035	2990–2806	1612–1415	1250–1089	856–524	-	433

theoretical studies were performed via the LanL2DZ based DFT/B3LYP method. The results of the theoretical calculations indicate that the N-H and C-H stretching vibrations should appear in the ranges 3570–3357 and 3135–3092 cm^{-1}, respectively. The vibrational bands for C-Br, Pd-Cl and Pd-N, which are characteristic for this complex, were observed to lie in the fingerprint region. The theoretical potential energy distribution (%PED) showed that the vibrational bands of C=C, C=N and C-C overlapped. For the $[PdCl_2L^3_2]$ complex, the calculation showed that the C-H stretching vibrations were to appear in the range 3363–2965 cm^{-1}. These bands were observed as medium and weak intensity bands in the FTIR spectra. The vibrational bands conferred to the in-plane C-C and C-H bending vibrations are presented in Table S1 in detail. For the $[PdCl_2L^4_2]$ complex, the C-H stretching vibrations of $[PdCl_2L^4_2]$—a structural isomer of the $[PdCl_2L^3_2]$ complex—were calculated to be in the range 3141–2918 cm^{-1}. The results of the calculations showed that while the in-plane C-H stretching bands would appear in the range 1520–1448 cm^{-1}, the C-H bending vibrations were to be observed in the range 1073–852 cm^{-1}. The Pd-Cl stretching vibration, which is characteristic for this complex, was calculated to appear at 415 and 409 cm^{-1}. The obtained experimental and theoretical results are compatible with each other.

3.3. Molecular geometry studies

The optimized bond lengths and bond angles of the complexes are given in Table S2. Mainly five different bond lengths were observed in common for the C-C, C-H, C-N, N-Pd, and Pd-Cl bonds for these complexes. The length of the Pd-Cl and Pd-N bonds for all of the four complexes were calculated to be the same and are 2.27 and 2.05 Å, respectively. When all the bond lengths were examined, the longest bond length was determined to be the one between the palladium and the chlorine atoms. For the $[PdCl_2L^1_2]$ complex, the shortest bond length, which was calculated to be 0.96 Å, was observed to belong to the O-H bond. In other complexes, the length of the bond between the carbon and hydrogen atoms was calculated to be 1.07 Å. It can be seen in Table S2, the bonding angles between the Cl-Pd-Cl, Cl-Pd-N and N-Pd-N atoms are 90°. These bonding angles are the smallest for all the four complexes.

3.4. NMR studies

The ^{1}H-NMR and ^{13}C-NMR spectra of the complexes obtained in DMSO, which was used as the solvent, are presented in Table 2. The results of the theoretical calculations are presented in Table S3 in detail.

In the ^{1}H-NMR spectrum of the $[PdCl_2L^1_2]$ complex, the multiple peaks observed in the range 8.64–7.42 ppm can be attributed to the Ar-H (16 H) peaks in the Py ring. The peaks observed at 4.24 ppm indicate the Al-H protons (4 H). The theoretical ^{1}H-NMR values for this complex were calculated to be in the range 9.48–4.07 ppm.

In the ^{13}C-NMR spectrum, the peak observed at 152.5 ppm shows the two C atoms of the complex in the o-position. The peak observed at 149.4 ppm shows the two C atoms in the p-position and the peak at 146.0 ppm shows the two C atoms to which the nitro group in the phenyl ring is bound. The other peak observed at 146.2 ppm indicates the two C atoms via which the phenyl ring is bound to the -CH_2 bridge. The peak observed at 130.1 ppm indicates the four C atoms of the aromatic carbon in the phenyl ring. The peak at 125.3 ppm indicates the four C atoms in the metaposition. The peak at 123.6 ppm shows the four C atoms in the other aromatic carbon in the phenyl ring. The peak at 40.0 ppm indicates the two C atoms in the aliphatic groups of the complex. When these results are compared with the theoretical data it was seen that these values were distributed in the range 163–50 ppm and the chemical shifts observed in the ^{13}C-NMR spectra of the structures were >100 ppm as expected according to the calculations.

The multiple peaks observed in the range 8.76–6.14 ppm in the ^{1}H-NMR spectrum of the $[PdCl_2L^2_2]$ complex show the Ar-H (6 H) peaks in the Py ring. The singlet peak observed at 7.64 ppm shows the protons (4 H) in the amine group. In the ^{13}C-NMR spectrum of the complex, the peak belonging to the two C atoms in the amine group at the o-position of the ring was observed at 158.1 ppm. The peak for the two C atoms in the other o-position was observed at 149.3 ppm. The peak for the two C atoms in the p-position was observed at 140.5 ppm. The peak for the two C atoms in the m-position was observed at 112.3 ppm. The peak observed at 103.5 ppm shows the two C atoms in the halogen groups of the complex.

Table 2. The ^{1}H-NMR and ^{13}C-NMR data for the complexes.

Complexes	Ar-H ppm	Al-H ppm	N-H Ppm	Ar-C ppm	Al-C ppm
$[PdCl_2L^1_2]$	8.64–7.42	4.24	-	152–123	40.00
$[PdCl_2L^2_2]$	8.76–6.14	-	7.64	158–103	-
$[PdCl_2L^3_2]$	8.40–7.65	3.31–2.26	-	150–133	17.88
$[PdCl_2L^4_2]$	8.45–7.30	3.31–2.24	-	151–134	18.54

The multiple peaks observed in the range 8.40–7.65 ppm in the ^{1}H-NMR spectrum of the [$PdCl_2L^3_2$] belong to the Ar-H (6 H) in the Py ring. These values were calculated to be in the range 9.76–7.99 ppm theoretically. The peaks observed in the range 3.31–2.26 ppm indicate the protons (12 H) in the methyl group. Theoretically they were found to be in the range 5.96–1.37 ppm.

In the ^{13}C-NMR spectrum, the peak observed at 150.2 ppm shows the four C atoms in the o-position. The peak of the two C atoms in the para position was observed at 140.6 ppm. The peak observed at 134.9 ppm indicates the four C atoms in the m-position. The peak at 17.9 ppm shows the four C atoms in the methyl groups. Theoretically they were calculated to be in the 174.51–26.77 ppm range.

In the ^{1}H-NMR spectrum of the [$PdCl_2L^4_2$] complex, the multiple peaks observed in the range 8.45–7.30 ppm indicate the Ar-H (6 H) peaks in the Py ring. The peaks observed in the range 3.31–2.24 ppm indicate the protons (12 H) in the methyl group.

In the ^{13}C-NMR spectrum, the peak observed at 151.5 ppm shows the four C atoms in the o-position. The peak at 149.9 ppm shows the two C atoms in the p-position. The peak at 134.2 ppm indicates the four C atoms in the m-position. The peak at 18.5 ppm shows the four C atoms in the methyl group.

3.5. Investigation of the MEP surface and Mulliken charge distribution

Molecular electrostatic potential surface maps (MEP), which allow us to observe the variable charge region, show the charge distributions of molecules in three dimensions.

Mulliken atomic charge distributions of the complexes are given in Table 3. Figure 1 shows that the MEP surfaces of the complexes range from the darkest red to the darkest blue. Blue, red, and green colors indicate nucleophilicity, electrophilicity, and hydrogen bond interactions (regions of neutral or zero electrostatic potential), respectively [29,30].

In the MEP map, it is observed that the negative potential regions in the molecule are concentrated on oxygen and chlorine atoms. Complexes with such active sites generally show good biological activity. The Mulliken population analysis was performed in detail and the relevant results are given in Figure 1.

3.6. Investigation of the frontier molecular orbitals (FMOs) and the chemical reactivity

The difference between HOMO and LUMO energies determines the chemical reactivity and kinetic stability of a molecule. Moreover, with the calculated HOMO-LUMO values, the polarization, electronegativity, hardness, and reactivity of the energy gap molecule can be determined. The surface images are presented in Figure 2. The chemical reactivity indices are given in Table 4. A smaller HOMO-LUMO energy deficiency can indicate greater biological activity [31,32]. For the [$PdCl_2L^1_2$], [$PdCl_2L^2_2$], [$PdCl_2L^3_2$], [$PdCl_2L^4_2$] complexes while the HOMO energies were calculated to be –5.83, –6.43, –5.60 and –5.77 eV; the LUMO energies were calculated to be –2.08, –2.55, –1.88, and –1.99 eV, respectively. Also, the energy gap between the HOMO and LUMO orbitals were calculated to be 3.75, 3.88, 3.72 and 3.78, respectively.

3.7. Investigation of the cytotoxicity

The effect of the complexes on cell proliferation of the HepG2 cells was investigated via MTT Assay. Half maximal inhibitory concentrations (IC50) of complexes were determined according to the MTT Assay results. IC50 values of [$PdCl_2L^1_2$], [$PdCl_2L^2_2$], [$PdCl_2L^3_2$] and [$PdCl_2L^4_2$] complexes were found to be 498.69 μmol L^{-1}, 157.21 μmol L^{-1}, 216.5 μmol L^{-1} and 61.04 μmol L^{-1}, respectively. The change in cell viability was observed to be concentration dependent and also was affected from the structure of the complexes. HepG2 cells were interacted with complex solutions of different concentrations (3.12, 6.25, 12.5, 25, 50, 100, and 200 μmol L^{-1}). The proliferation of the HepG2 cell line is suppressed depending on the added complex dose. Moreover, as can be seen in Figure 3, the data obtained from the cell viability study indicated that bis(dichlorobis(3,4-dimethylpyridine) palladium(II), [$PdCl_2L^4_2$] was the most cytotoxic complex and bis(4-(4-nitrobenzyl)pyridine)dichloropalladium(II), [$PdCl_2L^1_2$] was the least cytotoxic. In recent years, the cytotoxic activities of many types of complexes against various cancer cell lines have been studied. Among them palladium complexes (II) with 2,2′-bipyridine (bpy) ligands were found to be cytotoxic against colorectal adenocarcinoma and breast cancer cell lines [20]. In addition cytotoxic activity of palladium(II) complexes with 2,6-dimethyl-4-nitropyridine complexes and palladium(II) with 4,4′-bipyridine ligands were observed against several cancer cell lines in a dose-dependent manner [21, 22]. In this research, each complex suppressed the proliferation of HepG2 cell line in a dose-dependent manner with parallel to similar studies in the literature.

3.8. Investigation of the effect of complexes on cell injury

Cell injury was investigated via LDH assay conducted in culture media since LDH is a stable cytosolic enzyme in normal cells and when membrane damage occurs it leaks into the extracellular fluid. According to the cell viability assay bis(dichlorobis(3,4-dimethylpyridine) palladium(II), [$PdCl_2L^4_2$] was the most cytotoxic complex and this complex increased LDH release—a cell damage marker—remarkably. The LDH release caused by bis(2-amino-5-bromopyridine)

Table 3. Mulliken atomic charge of the complexes.

$[PdCl_2L^1_2]$		$[PdCl_2L^2_2]$		$[PdCl_2L^3_2]$		$[PdCl_2L^4_2]$	
Atom	**Mulliken atomic charge**	**Atom**	**Mulliken atomic charge**	**Atom**	**Mulliken atomic charge**	**Atom**	**Mulliken atomic charge**
1Pd	–0.053	1Pd	0.061	1Pd	–0.094	1Pd	–0.055
2Cl	–0.244	2Cl	–0.245	2Cl	–0.244	2Cl	–0.247
3Cl	–0.244	3Cl	–0.246	3Cl	–0.241	3Cl	–0.247
4C	–0.101	4C	–0.095	4C	–0.134	4C	–0.101
5C	–0.113	5C	0.238	5C	0.351	5C	–0.207
6C	–0.318	6C	–0.181	6C	–0.336	6C	–0.330
7H	0.245	7H	0.271	7H	0.244	7H	0.247
8C	–0.303	8C	–0.261	8C	–0.427	8C	0.253
9H	0.259	9C	–0.056	9C	0.419	9H	0.264
10C	0.478	10H	0.247	10H	0.233	10C	0.289
11H	0.227	11H	0.253	11H	0.241	11H	0.234
12H	0.226	12C	0.235	12C	0.380	12C	–0.231
13C	–0.106	13C	–0.100	13C	–0.139	13C	–0.107
14C	–0.112	14C	–0.262	14C	–0.423	14C	0.255
15C	–0.307	15C	–0.179	15C	–0.327	15H	0.257
16H	0.252	16H	0.280	16H	0.253	16C	–0.330
17C	–0.312	17C	–0.054	17C	0.416	17H	0.257
18H	0.254	18H	0.245	18H	0.240	18C	0.304
19C	0.478	19H	0.253	19H	0.234	19H	0.235
20H	0.227	20N	–0.256	20N	–0.286	20N	–0.253
21H	0.227	21N	–0.255	21N	–0.290	21N	–0.252
22N	–0.260	22N	–0.532	22C	–0.690	22C	–0.767
23N	–0.260	23H	0.304	23H	0.202	23H	0.245
24C	–0.673	24H	0.264	24H	0.292	24H	0.241
25H	0.213	25N	–0.550	25H	0.211	25H	0.230
26H	0.209	26H	0.266	26C	–0.731	26C	–0.757
27C	–0.673	27H	0.313	27H	0.299	27H	0.228
28H	0.212	28Br	0.020	28H	0.231	28H	0.236
29H	0.211	29Br	0.022	29H	0.222	29H	0.222
30C	0.520			30C	–0.735	30C	–0.749
31C	–0.367			31H	0.225	31H	0.235
32C	–0.367			32H	0.239	32H	0.227
33C	–0.361			33H	0.218	33H	0.229
34H	0.213			34C	–0.735	34C	–0.739
35C	–0.359			35H	0.241	35H	0.235
36H	0.213			36H	0.223	36H	0.226
37C	0.386			37H	0.219	37 H	0.221
38H	0.255						
39H	0.255						
40C	0.520						

Table 3. (Continued).

41C	–0.366						
42C	–0.366						
43C	–0.360						
44H	0.213						
45C	–0.360						
46H	0.213						
47C	0.386						
48H	0.254						
49H	0.256						
50N	–0.048						
51N	–0.047						
52O	–0.428						
53H	0.346						
54O	–0.434						
55H	0.355						
56O	–0.428						
57H	0.346						
58O	–0.434						
59H	0.355						

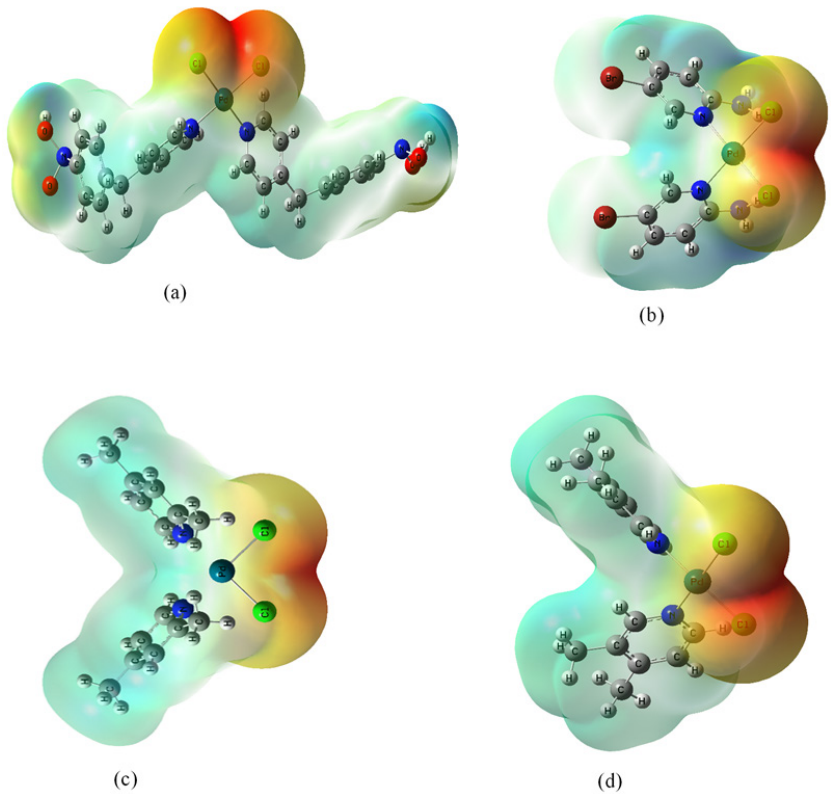

Figure 1. The colored coded picture of the electrostatic potential surface of the complexes (a) $PdCl_2L^1{}_2$, (b) $PdCl_2L^2{}_2$, (c) $PdCl_2L^3{}_2$, (d) $PdCl_2L^4{}_2$.

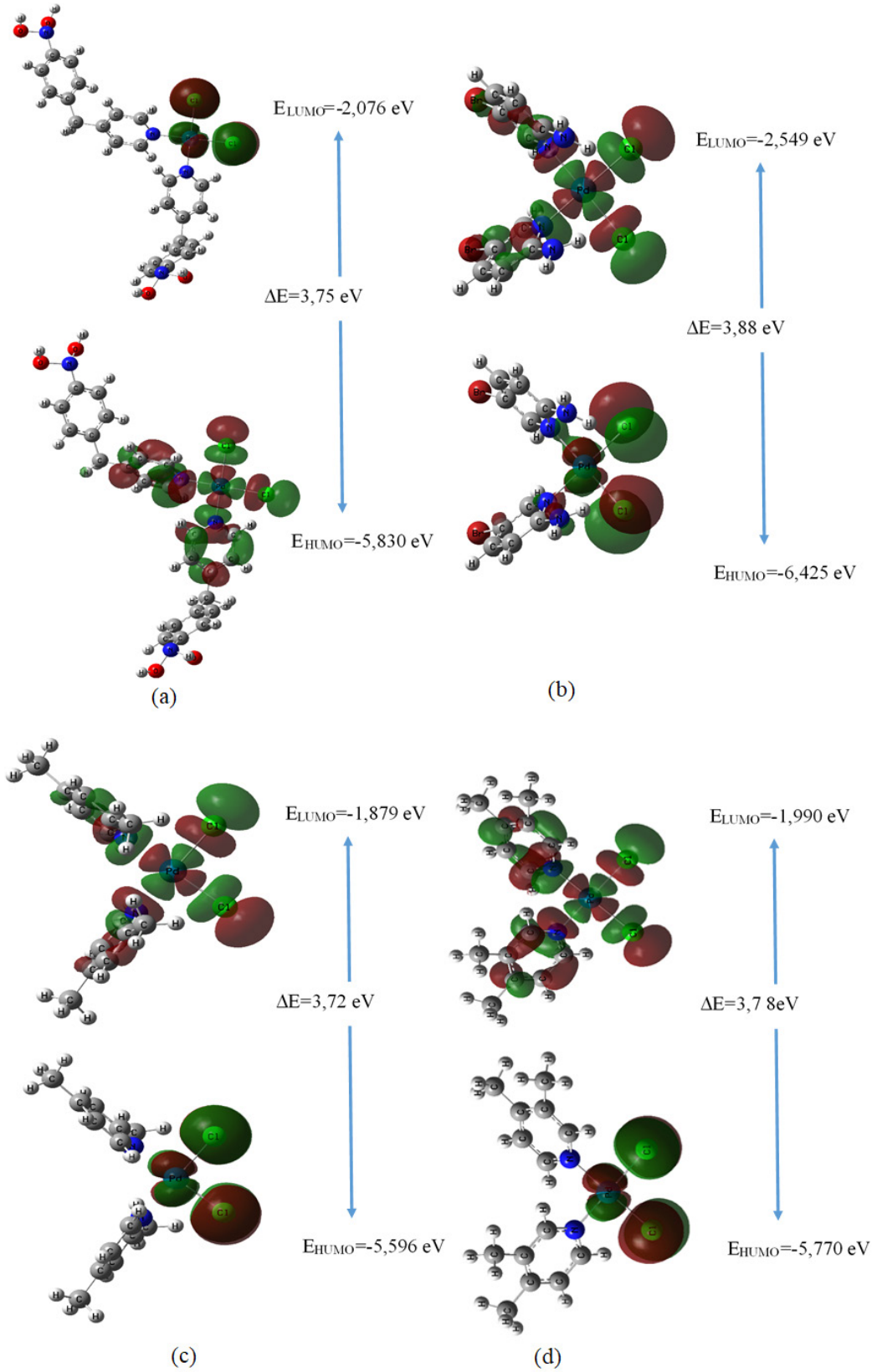

Figure 2. The HOMO and the LUMO surface images of the complexes (a) $[PdCl_2L^1_2]$, (b) $[PdCl_2L^2_2]$, (c) $[PdCl_2L^3_2]$, (d) $[PdCl_2L^4_2]$.

Table 4. Some global reactivity properties of the complexes.

Parameters	**[PdCl2L12] (eV)**	**[PdCl2L22] (eV)**	**[PdCl2L32] (eV)**	**PdCl2L42] (eV)**
E_{HOMO}	–5.83	–6.43	–5.60	–5.77
E_{LUMO}	–2.08	–2.55	–1.88	–1.99
DE	3.75	3.88	3.72	3.78
Ionization potential ($I = -E_{HOMO}$)	5.83	6.43	5.60	5.77
Electron affinity ($A = -E_{LUMO}$)	2.08	2.55	1.88	1.99
Electronegativity ($\chi = (I+A)/2$)	6.05	4.49	3.74	3.88
Chemical potential ($\mu = -(I+A)/2$)	–6.05	–4.49	–3.74	–3.88
Chemical hardness ($\eta = (I-A)/2$)	1.877	1.94	1.86	1.89
Chemical softness ($s = 1/2\eta$)	0.266	0.26	0.27	0.27
Electrophilic index ($w = \mu^2/2\eta$)	9.74	5.19	3.76	3.98
Maximum load transfer parameter ($\Delta N_{max} = (I+A)/2(I-A)$)	1.05	1.16	1.01	1.03

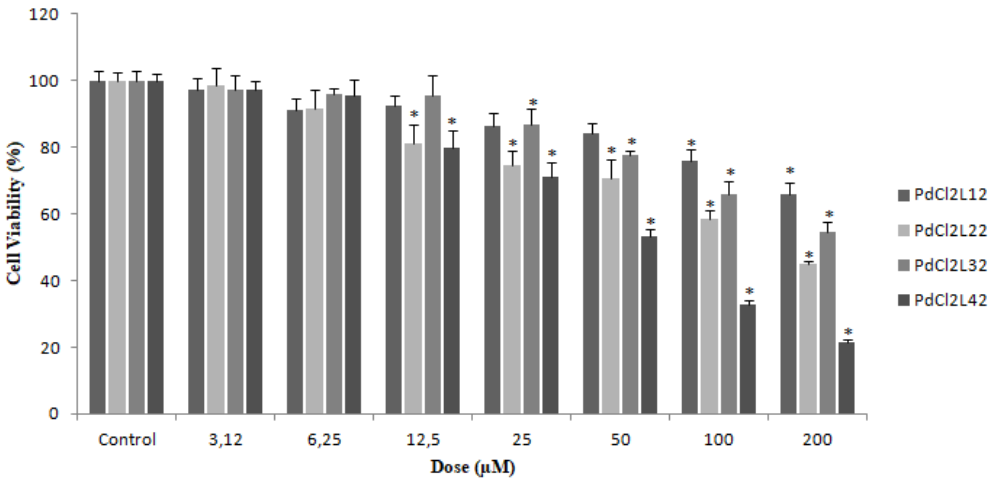

Figure 3. Viability of HepG2 cells treated with different doses of the complexes for 24 h. (*$p < 0.05$ indicates the significance of difference as compared with that of the control).

dichloropalladium(II), $[PdCl_2L^2_2]$ complex was the second highest among all the complexes studied. The LDH concentration (IU/mL) in the supernatant is given in Figure 4.

3.9. Molecular docking studies

The molecular docking technique describes the interactions between drug and enzyme and is therefore used in drug design studies [33]. Pd-based drugs are used in treatment of various cancers [34,35]. In this study, the interaction mechanism between the synthesized palladium complexes and the 2OH4 encoded HepG2 protein was investigated. The 3D crystal structure of the protein (PDB ID: 2OH4) targeted for HepG2 was observed using the RSBC PDB format.

The DFT/B3LYP/LanL2DZ basis set was used to optimize the structures of the synthesized complexes. The interaction energies between the complexes and the protein arise from the hydrogen bonds and van der Waals interactions and confer stability to the complex. According to the results of the molecular docking studies, which are given in Figure 5, the protein-ligand interactions for the synthesized complexes were between the active residues in the 2OH4 protein and the H and Cl atoms of the ligands. It was observed that the synthesized complexes interacted with a few residue of the 2OH4 protein. While the $[PdCl_2L^1_2]$ complex interacted with the PRO-1105, HIS-1142, ARG-1122, ALA1125, MET-1123 residues, the $[PdCl_2L^2_2]$ complex interacted with the LYS-824, LEU-900, LEU-899, HIS-892, ASN-898 residues. In a similar way, the $[PdCl_2L^3_2]$ complex interacted with the GLU-1036, PHE-916, LYS-918, ARG-861, THR-862 residues and the $[PdCl_2L^4_2]$ complex interacted with the GLY-1061, ALA-1063, SER-923, LEU-1065, SER-1102 residues.

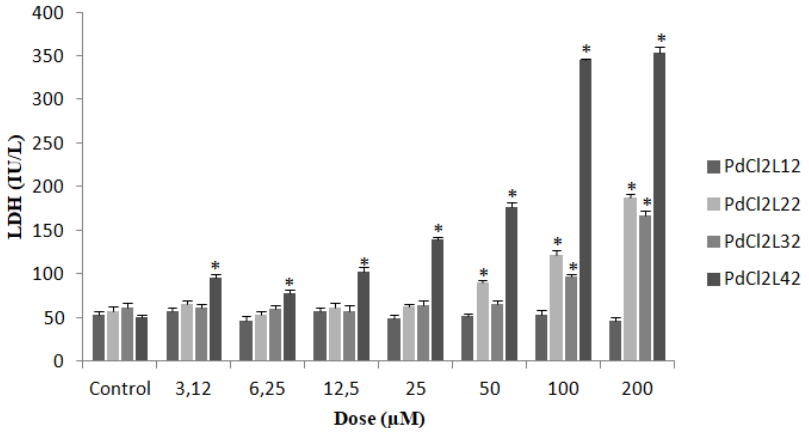

Figure 4. Cell culture supernatant lactate dehydrogenase (LDH) levels after 24-h incubation period. (*p < 0.05 indicates the significance of difference as compared with that of the control).

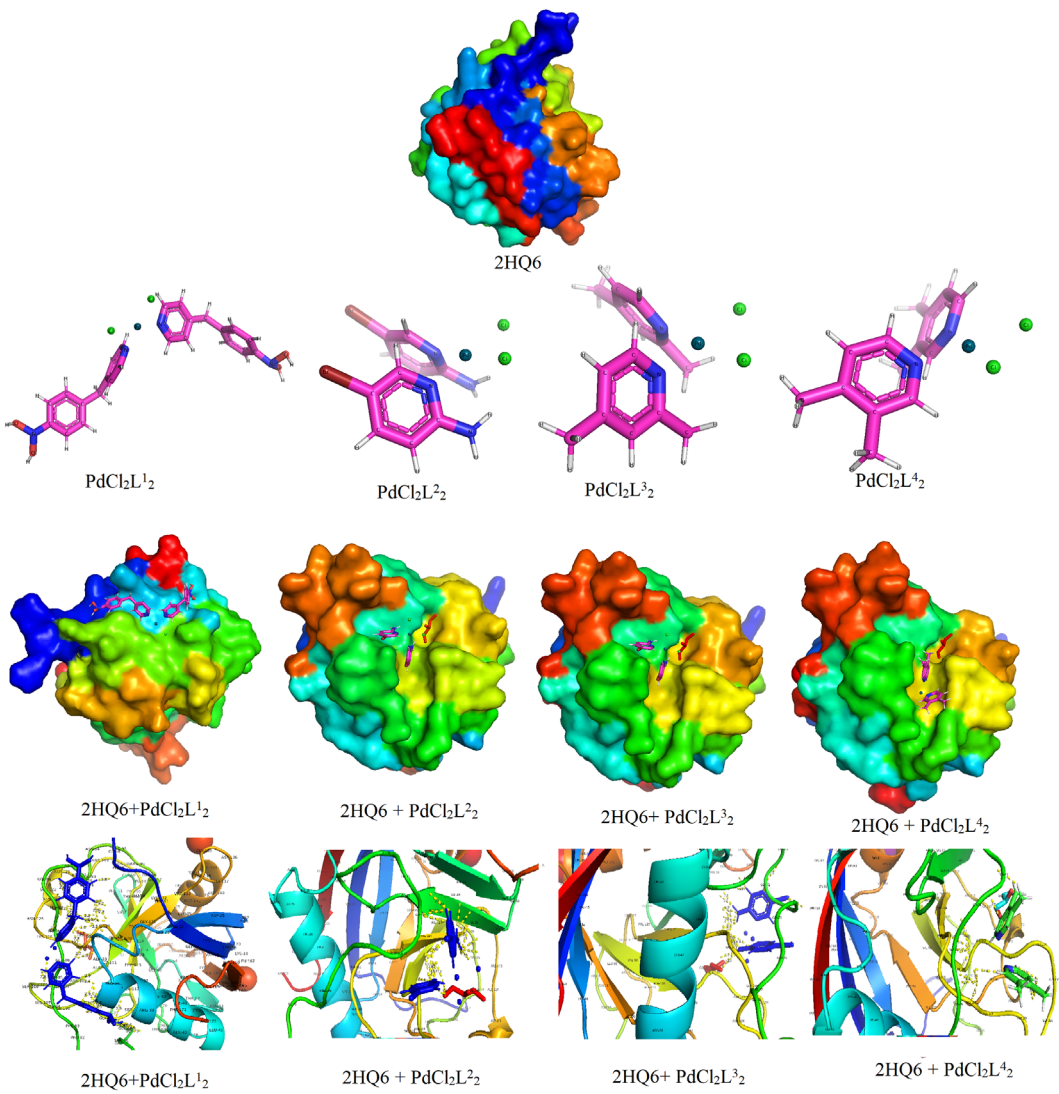

Figure 5. Docking diagram of the 2HQ6 target protein and the complex-protein interactions

4. Conclusion

Currently, drug resistance is developing in cancer treatment and side effects of chemotherapy are frequently observed. Therefore, synthesis of new and effective chemotherapy agents has profound importance. In this study, novel bis(4-(4-nitrobenzyl)pyridine)dichloropalladium(II), $[PdCl_2L^1_2]$, bis(2-amino-5-bromopyridine)dichloropalladium(II), $[PdCl_2L^2_2]$, bis(2,4-dimethylpyridine)dichloropalladium(II), $[PdCl_2L^3_2]$, bis(3,4-dimethylpyridine)dichloropalladium(II), $[PdCl_2L^4_2]$ complexes were prepared. The spectroscopic techniques were used to characterization studies. In addition to experimental studies, theoretical calculations (molecular structures, potential energy distribution analysis, MEP, HOMO-LUMO orbitals and Mulliken charge distribution) were also made. Experimental results were supported by theoretical calculations. The study on the antiproliferative effects of these complexes on hepatocellular carcinoma cells (HepG2) was carried out. In our study, it was observed that the synthesized complexes had a different antiproliferative effect. According to the MTT results, the $[PdCl_2L^4_2]$ and $[PdCl_2L^2_2]$ complexes were found to be very effective even at low concentrations. The data obtained in the cell injury study were compatible with these results. This indicated that palladium complexes with pyridine ligands have antiproliferative activities on HepG2 cells. The cell based studies conducted indicated that the synthesized novel palladium complexes had cytotoxic effects on HepG2 cell line and the $[PdCl_2L^4_2]$ complex was found to be the most effective among all other complexes studied.

The interaction mechanisms between the complexes and the liver cancer protein were investigated via molecular docking. The study on the antiproliferative effects of these complexes on hepatocellular carcinoma cells (HepG2) showed that they are potent candidates for use against this liver cancer cell line. In vivo studies would allow better understanding of the metabolic effects of these compounds.

Conflict of interest

The authors declare no conflict of interest.

Acknowledgments

This study was supported by Burdur Mehmet Akif Ersoy University BAP under project number of 0232-YL-14.

References

1. Kocyigit UM, Budak Y, Gürdere MB, Tekin Ş, Köprülü TK et al. Synthesis, characterization, anticancer, antimicrobial and carbonic anhydrase inhibition profiles of novel (3aR, 4S, 7R, 7aS)-2-(4-((E)-3-(3-aryl) acryloyl) phenyl)-3a, 4, 7, 7a-tetrahydro-1H-4, 7-methanoisoindole-1, 3 (2H)-dione derivatives. Bioorganic Chemistry 2017; 70: 118-125.
2. Dastan T, Kocyigit UM, Durna Dastan S, Canturk Kilickaya P, Taslimi P et al. Investigation of acetylcholinesterase and mammalian DNA topoisomerases, carbonic anhydrase inhibition profiles, and cytotoxic activity of novel bis (α-aminoalkyl) phosphinic acid derivatives against human breast cancer. Journal of Biochemical and Molecular Toxicology, 2017; 31 (11): e21971.
3. Global Cancer Observatory. Accessed August 25, 2020. https://gco.iarc.fr/
4. Kumar V, Abbas AK, Aster JC. Robbins and Cotran Pathologic Basis of Disease. Saunders; 2015. Accessed December 29, 2021. http://vlib.kmu.ac.ir/kmu/handle/kmu/87089
5. Global Cancer Observatory. Accessed December 29, 2021. https://gco.iarc.fr/
6. Morales-Cruz M, Delgado Y, Castillo B et al. Smart targeting to improve cancer therapeutics. Drug Design, Development and Therapy 2019; 13: 3753-3772. https://doi.org/10.2147/DDDT.S219489
7. Lewandowska AM, Lewandowski T, Rudzki M, Rudzki S, Laskowska B. Cancer prevention – review paper. Annals of Agricultural and Environmental Medicine 2021; 28 (1): 11-19. https://doi.org/10.26444/AAEM/116906
8. Nakashima L. Evolution of cancer treatment and evolving challenges. Healthcare Management Forum 2018; 31 (1): 26-28. https://doi.org/10.1177/0840470417722568
9. Mollaei M, Hassan ZM, Khorshidi F, Langroudi L. Chemotherapeutic drugs: Cell death- and resistance-related signaling pathways. Are they really as smart as the tumor cells? Translational Oncology 2021; 14 (5): 101056. https://doi.org/10.1016/J.TRANON.2021.101056
10. Ndagi U, Mhlongo N, Soliman ME. Metal complexes in cancer therapy – An update from drug design perspective. Drug Design, Development and Therapy 2017; 11: 599-616. https://doi.org/10.2147/DDDT.S119488
11. Simpson P V., Desai NM, Casari I, Massi M, Falasca M. Metal-based antitumor compounds: beyond cisplatin. Future Medicinal Chemistry 2019; 11 (2): 119-135. https://doi.org/10.4155/FMC-2018-0248

12. Fanelli M, Formica M, Fusi V, Giorgi L, Micheloni M, Paoli P. New trends in platinum and palladium complexes as antineoplastic agents. Coordination Chemistry Reviews 2016; 310: 41-79. https://doi.org/10.1016/J.CCR.2015.11.004

13. Carneiro TJ, Martins AS, Marques MPM, Gil AM. Metabolic aspects of palladium(II) potential anti-cancer drugs. Frontiers in Oncology 2020; 10. https://doi.org/10.3389/FONC.2020.590970

14. Kapdi AR, Fairlamb IJS. Anti-cancer palladium complexes: a focus on PdX2L2, palladacycles and related complexes. Chemical Society Reviews 2014; 43 (13): 4751-4777. https://doi.org/10.1039/C4CS00063C

15. Boopalachandran P, Sheu HL, Laane J. Vibrational spectra, structure, and theoretical calculations of 2-chloro- and 3-chloropyridine and 2-bromo- and 3-bromopyridine. Journal of Molecular Structure 2012; 1023: 61-67. https://doi.org/10.1016/J.MOLSTRUC.2012.03.031

16. Mock C, Puscasu I, Rauterkus MJ, Tallen G, Wolff JEA et al. Novel Pt(II) anticancer agents and their Pd(II) analogues: syntheses, crystal structures, reactions with nucleobases and cytotoxicities. Inorganica Chimica Acta 2001; 319 (1-2): 109-116. https://doi.org/10.1016/S0020-1693(01)00459-5

17. Allan JR, Carson BR, Gerrard DL, Birnie J. Thermal, spectral and magnetic studies of some first row transition metal complexes of 2-(p-tolyl) pyridine. Thermochimica Acta 1990; 160 (2): 329-335. https://doi.org/10.1016/0040-6031(90)80273-2

18. Frej A, Goeschen C, Näther C, Lüning U, Herges R. Synthesis and properties of di- and trinitrobenzyl substituted pyridine derivates. The paper is supposed to be published in the special issue of the ESOR XII 2009 meeting in Haifa. Editor of the issue is Amnon Stanger. Journal of Physical Organic Chemistry 2010; 23 (11): 1093. https://doi.org/10.1002/POC.1781

19. Kismali G, Emen FM, Yesilkaynak T, Meral O, Demirkiran D et al. The cell death pathway induced by metal halide complexes of pyridine and derivative ligands in hepatocellular carcinoma cells-necrosis or apoptosis. European Review for Medical and Pharmacological Sciences 2012; 16 (8): 1001-1012.

20. Tabrizi L, Zouchoune B, Zaiter A. Theoretical and experimental study of gold(III), palladium(II), and platinum (II) complexes with 3-((4-nitrophenyl)thio)phenylcyanamide and 2,2′-bipyridine ligands: Cytotoxic activity and interaction with 9-methylguanine. Inorganica Chimica Acta 2020; 499: 119211. https://doi.org/10.1016/J.ICA.2019.119211

21. Kuduk-Jaworska J, Puszko A, Kubiak M, Pelczyńska M. Synthesis, structural, physico-chemical and biological properties of new palladium(II) complexes with 2,6-dimethyl-4-nitropyridine. Journal of Inorganic Biochemistry 2004; 98(8): 1447-1456. https://doi.org/10.1016/J.JINORGBIO.2004.05.008

22. Franich AA, Živković MD, Milovanović J, Arsenijević D, Arsenijević A et al. In vitro cytotoxic activities, DNA- and BSA-binding studies of dinuclear palladium(II) complexes with different pyridine-based bridging ligands. Journal of Inorganic Biochemistry. 2020; 210: 111158. https://doi.org/10.1016/J.JINORGBIO.2020.111158

23. M.J Frisch, Trucks GW, Schlegel HB, Suzerain GE, Robb MA et al. Gaussian 09. Published online 2003.

24. Abkari A, Chaabane I, Guidara K. DFT (B3LYP/LanL2DZ and B3LYP/6311G+(d,p)) comparative vibrational spectroscopic analysis of organic-inorganic compound bis(4-acetylanilinium) tetrachlorocuprate(II). Physica E: Low-Dimensional Systems and Nanostructures 2016; 81: 136-144. https://doi.org/10.1016/j.physe.2016.03.010

25. Dennington R, Keith JM. Gausswiev 5. Published online 2009.

26. Jamroz MH. Vibrational Energy Distribution Analysis VEDA 4. Published online 2004.

27. Ritchie DW. Evaluation of protein docking predictions using Hex 3.1 in CAPRI rounds 1 and 2. Proteins: Structure, Function, and Bioinformatics 2003; 52 (1): 98-106. https://doi.org/10.1002/PROT.10379

28. Delano LW. The PyMOL Molecular Graphics System. http://www.pymol.org. Published online 2002. Accessed September 11, 2021. https://ci.nii.ac.jp/naid/10020095229

29. Alam M, Park S. Molecular structure, spectral studies, NBO, HOMO-LUMO profile, MEP and Mulliken analysis of 3β,6β-dichloro-5α-hydroxy-5α-cholestane. Journal of Molecular Structure 2018; 1159: 33-45. https://doi.org/10.1016/J.MOLSTRUC.2018.01.043

30. Demircioğlu Z, Kaştaş ÇA, Büyükgüngör O. Theoretical analysis (NBO, NPA, Mulliken Population Method) and molecular orbital studies (hardness, chemical potential, electrophilicity and Fukui function analysis) of (E)-2-((4-hydroxy-2-methylphenylimino)methyl)-3-methoxyphenol. Journal of Molecular Structure 2015; 1091: 183-195. https://doi.org/10.1016/j.molstruc.2015.02.076

31. Franco-Pérez M, Gázquez JL. Electronegativities of Pauling and Mulliken in Density Functional Theory. Journal of Physical Chemistry A. 2019; 123(46): 10065-10071. https://doi.org/10.1021/ACS.JPCA.9B07468/SUPPL_FILE/JP9B07468_SI_001.PDF

32. Kutlu E, Emen FM, Kismali G et al. Pyridine derivative platinum complexes: Synthesis, molecular structure, DFT and initial anticancer activity studies. Journal of Molecular Structure 2021; 1234: 130191. https://doi.org/10.1016/j.molstruc.2021.130191

33. Celik S, Albayrak AT, Akyuz S, Ozel AE. Synthesis, molecular docking and ADMET study of ionic liquid as anticancer inhibitors of DNA and COX-2, TOPII enzymes. Journal of Biomolecular Structure & Dynamics 2020; 38 (5): 1354-1364. https://doi.org/10.1080/07391102.2019.1604263

34. Farhangian H, Eslami Moghadam M, Divsalar A, Rahiminezhad A. Anticancer activity of novel amino acid derivative of palladium complex with phendione ligand against of human colon cancer cell line. Journal of biological inorganic chemistry : JBIC : a publication of the Society of Biological Inorganic Chemistry 2017; 22 (7): 1055-1064. https://doi.org/10.1007/S00775-017-1483-Y

35. Pranczk J, Jacewicz D, Wyrzykowski D, Chmurzynski L. Platinum(II) and Palladium(II) Complex Compounds as Anti-cancer Drugs. Methods of Cytotoxicity Determination. Current Pharmaceutical Analysis 2014; 10 (1): 2-9.

Table S1. Detailed assignments of experimental and theoretical wavenumbers (cm^{-1}) of the complexes along with potential energy distribution (PED).

$[PdCl_2L^1{}_2]$			*$[PdCl_2L^2{}_2]$*			*$[PdCl_2L^3{}_2]$*			*$PdCl_2L^4{}_2$*		
B3LYP\ LanL2dz	Scaled	Assignment	B3LYP\ LanL2dz	Scaled	Assignment	B3LYP\ LanL2dz	Scaled	Assignment	B3LYP\ LanL2dz	Scaled	Assignment
3646	3500	$\nu_{(OH)}$99	3719	3570	$\nu_{(NH)}$95	3503	3363	ν(CH)84	3272	3141	ν(CH)94
3643	3497	$\nu_{(OH)}$84	3713	3564	$\nu_{(NH)}$83	3400	3264	ν(CH)94	3260	3130	ν(CH)96
3272	3141	$\nu_{(CH)}$91	3517	3376	$\nu_{(NH)}$84	3396	3260	ν(CH)90	3255	3125	ν(CH)94
3262	3132	$\nu_{(CH)}$92	3497	3357	$\nu_{(NH)}$92	3395	3259	ν(CH)95	3241	3111	ν(CH)99
3260	3130	$\nu_{(CH)}$97	3266	3135	$\nu_{(CH)}$90	3394	3258	ν(CH)96	3225	3096	ν(CH)95
3257	3127	$\nu_{(CH)}$97	3258	3128	$\nu_{(CH)}$89	3391	3255	ν(CH)80	3220	3091	ν(CH)90
3254	3124	$\nu_{(CH)}$89	3244	3114	$\nu_{(CH)}$93	3301	3169	ν(CH)94	3152	3026	ν(CH)80
3233	3104	$\nu_{(CH)}$89	3223	3094	$\nu_{(CH)}$94	3277	3146	ν(CH)92	3145	3019	ν(CH)79
3220	3091	$\nu_{(CH)}$95	3221	3092	$\nu_{(CH)}$94	3272	3141	ν(CH)92	3111	2987	ν(CH)99
3216	3087	$\nu_{(CH)}$91	1696	1696	$\delta_{(HNH)}$74	3117	2992	ν(CH)89	3108	2984	ν(CH)88
3197	3069	$\nu_{(CH)}$90	1688	1688	$\delta_{(HNH)}$77	3115	2990	ν(CH)95	3041	2919	ν(CH)99
3191	3063	$\nu_{(CH)}$90	1650	1650	$\nu_{(CC)}$24+$\delta_{(HNH)}$10	3093	2969	ν(CH)96	3040	2918	ν(CH)99
3087	2964	$\nu_{(CH)}$98	1648	1648	$\nu_{(CC)}$35	3089	2965	ν(CH)89	1654	1654	$\nu_{(CC)}$57
3042	2920	$\nu_{(CH)}$98	1590	1590	$\nu_{(CC)}$24+$\nu_{(NC)}$19	1682	1682	$\nu_{(CC)}$42+$\delta_{(HCC)}$10	1601	1601	$\nu_{(CC)}$19+$\nu_{(NC)}$26+ $\delta_{(CCC)}$10+$\delta_{(CCN)}$21
1662	1662	$\nu_{(CC)}$57+$\delta_{(HCC)}$36	1589	1589	$\nu_{(CC)}$32+$\nu_{(NC)}$19	1631	1631	$\nu_{(CC)}$34+ $\nu_{(NC)}$12+ $\delta_{(CCC)}$12+$\delta_{(CCN)}$11	1529	1529	$\delta_{(HCC)}$36+$\delta_{(HCH)}$12
1654	1654	$\nu_{(CC)}$59	1535	1535	$\nu_{(NC)}$22+$\delta_{(HCC)}$40	1628	1628	$\nu_{(CC)}$12+ $\nu_{(NC)}$12+ $\delta_{(CCC)}$12	1520	1520	$\delta_{(HCH)}$64
1630	1630	$\nu_{(CC)}$63 +$\delta_{(CCC)}$10	1530	1530	$\nu_{(NC)}$22+$\delta_{(HCC)}$12	1600	1600	$\delta_{(HCH)}$58	1511	1511	$\delta_{(HCH)}$58
1593	1593	$\nu_{(NC)}$54+$\delta_{(CCC)}$10	1433	1433	$\delta_{(HCC)}$19+$\nu_{(NC)}$19	1513	1513	$\delta_{(HCH)}$50+$\tau_{(HCCN)}$12	1508	1508	$\delta_{(HCH)}$78
1539	1539	$\delta_{(HCC)}$52+$\nu_{(CC)}$15+ $\delta_{(CCC)}$14+	1429	1429	$\delta_{(HCC)}$14+$\nu_{(NC)}$21+ $\nu_{(CC)}$16	1499	1499	$\nu_{(CC)}$11+$\delta_{(HCC)}$26	1460	1460	$\delta_{(HCH)}$69+$\delta_{(HCC)}$10
1527	1527	$\delta_{(HCC)}$53	1372	1345	$\delta_{(HNC)}$15+$\nu_{(NC)}$11+ $\delta_{(CNC)}$10	1497	1497	$\nu_{(CC)}$12+$\delta_{(HCC)}$30	1452	1452	$\nu_{(CC)}$28+$\delta_{(HCC)}$29
1508	1508	$\delta_{(HNH)}$84	1371	1344	$\nu_{(CC)}$31+$\delta_{(HNC)}$14+ $\delta_{(CCC)}$11	1488	1488	$\delta_{(HCH)}$15	1448	1448	$\delta_{(HCH)}$60
1460	1460	$\delta_{(HCC)}$61 +$\nu_{(CC)}$45	1358	1331	$\delta_{(HCC)}$78		1484	$\delta_{(HCH)}$34	1357	1330	$\nu_{(CC)}$17+$\delta_{(HCC)}$55
1395	1367		1350	1323	$\delta_{(HCC)}$71		1478	$\delta_{(HCH)}$61+$\tau_{(HCCC)}$13	1321	1295	$\nu_{(CC)}$17+$\nu_{(NC)}$38
1384	1356	$\delta_{(HCC)}$17+ $\nu_{(CC)}$53	1324	1298	$\nu_{(NC)}$68	1484	1471	$\delta_{(HCH)}$50	1318	1292	$\nu_{(CC)}$19+$\nu_{(NC)}$37
1377	1349	$\delta_{(HON)}$78	1318	1292	$\nu_{(NC)}$61+$\delta_{(HCC)}$15	1478	1460	$\delta_{(HCH)}$50	1282	1256	$\nu_{(CC)}$48+$\delta_{(HCC)}$14
1359	1332	$\delta_{(HCC)}$63	1191	1167	$\delta_{(HCC)}$55	1471	1451	$\delta_{(HCH)}$26+ $\nu_{(CC)}$13	1236	1211	$\nu_{(CC)}$14+$\nu_{(NC)}$18+ $\delta_{(HCC)}$33
1306	1280	$\nu_{(NC)}$68	1190	1166	$\delta_{(HCC)}$57+ $\nu_{(CC)}$10	1460	1450	$\delta_{(HCH)}$18	1200	1176	$\nu_{(CC)}$10+$\nu_{(NC)}$10+$\delta_{(CCC)}$10 +$\delta_{(HCC)}$21+ $\delta_{(CCN)}$12
1296	1270	$\delta_{(HON)}$90	1115	1093	$\delta_{(HCC)}$14+ $\nu_{(CC)}$54	1451	1367	$\delta_{(HCH)}$91	1107	1085	$\nu_{(CC)}$17+$\nu_{(NC)}$40+ $\delta_{(HCC)}$14
1262	1237	$\nu_{(CC)}$12+$\delta_{(HCC)}$36	1110	1088	$\nu_{(CC)}$37	1450	1338	$\delta_{(HCH)}$90	1104	1082	$\nu_{(CC)}$16+$\nu_{(NC)}$43+$\delta_{(HCC)}$15

1240	1215	$\nu_{(CC)}13+ \nu_{(NC)}12 +\delta_{(HCC)}43$	1082	1060	$\delta_{(HNC)}53+ \nu_{(NC)}15$	1395	1328	$\delta_{(HCH)}19+\delta_{(HCC)}29$	1095	1073	$\tau_{(HCCC)}70$
1229	1204	$\nu_{(CC)}55$	1078	1056	$\delta_{(HNC)}50+\nu_{(NC)}13$	1365	1310	$\delta_{(HCH)}17+\delta_{(HCC)}32$	1072	1051	$\tau_{(HCCC)}46$
1221	1197	$\delta_{(HCC)}46+ \tau_{(HCCC)}12$	1045	1024	$\delta_{(CCC)}33+\delta_{(CCN)}13+\delta_{(CNC)}11$	1355	1249	$\nu_{(CC)}18+\nu_{(NC)}10+ \delta_{(CCC)}13+\delta_{(HCC)}11$	1039	1018	$\tau_{(HCCC)}36$
1206	1182	$\nu_{(CC)}14+ \nu_{(NC)}24 +\delta_{(HCC)}36$	1040	1019	$\delta_{(CCC)}34+\delta_{(CCN)}12+\delta_{(CNC)}10$	1337	1247	$\nu_{(CC)}17+\delta_{(CCC)}13$	1020	1000	$\tau_{(HCCC)}50$
1155	1132	$\nu_{(CC)}21+\delta_{(HCC)}57$	1007	987	$\tau_{(HCCC)}74$	1274	1212	$\nu_{(CC)}25+ \nu_{(NC)}19+ \delta_{(HCC)}21$	1005	985	$\tau_{(HCCC)}67+\tau_{(CCCN)}19$
1134	1111	$\nu_{(CC)}29+\delta_{(HCC)}25$	1006	986	$\tau_{(HCCC)}66+ \tau_{(CCCC)}14$	1272	1210	$\nu_{(CC)}24+ \nu_{(NC)}19+ \delta_{(HCC)}14$	948	929	$\tau_{(HCCC)}74$
1088	1066	$\delta_{(HCC)}29+\delta_{(CCN)}61$	948	929	$\tau_{(HCCC)}78$	1237	1166	$\nu_{(CC)}15+ \nu_{(NC)}11+ \delta_{(HCC)}14$	945	926	$\tau_{(HCCC)}58+\tau_{(CCNC)}12$
1048	1027	$\nu_{(NC)}46+ \delta_{(CCN)}11$	924	906	$\tau_{(HCCC)}75$	1235	1163	$\nu_{(NC)}10+ \delta_{(HCC)}22$	889	871	$\nu_{(CC)}32+\delta_{(CCN)}21$
1038	1017	$\delta_{(HCC)}15+ \delta_{(CCC)}69$	857	840	$\nu_{(NC)}17+\delta_{(CCC)}31$	1190	1110	$\nu_{(NC)}38+ \delta_{(CCN)}16$	869	852	$\tau_{(HCCC)}83$
1020	1000	$\tau_{(HCCC)}66+ \tau_{(CCNPd)}15$	855	838	$\delta_{(CCC)}44+ \nu_{(NC)}18$	1187	1108	$\nu_{(NC)}37+ \delta_{(CCN)}17$	765	750	$\delta_{(CCN)}33+\delta_{(CCC)}13+ \delta_{(CNC)}23$
1017	997	$\tau_{(HCCC)}55+ \tau_{(CNCC)}13$	850	833	$\tau_{(HCCC)}40+\gamma_{(CPdCN)}12$	1133	1059	$\tau_{(HCCN)}31+ \tau_{(CNCC)}10$	750	735	$\tau_{(CCNC)}19+ \tau_{(CCCN)}16$
1013	993	$\tau_{(HCCC)}47+ \tau_{(CCCN)}20$	848	831	$\tau_{(HCCC)}67+\gamma_{(CPdCN)}18$	1131	1040	$\tau_{(HCCC)}52$	749	734	$\tau_{(HCCC)}20+ \tau_{(CCCN)}16+ \tau_{(CCCC)}10$
1004	984	$\tau_{(HCCN)}70$	765	750	$\tau_{(HCCC)}13+\gamma_{(CPdCN)}15$	1081	1032	$\tau_{(HCCC)}43$	572	561	$\gamma_{(CCCC)}26+\gamma_{(CPdCN)}10$
923	905	$\nu_{(ON)}59+ \nu_{(OC)}10$	759	744	$\tau_{(HCCC)}12+\gamma_{(CPdCN)}34$	1061	1026	$\nu_{(CC)}11+\nu_{(NC)}28+ \delta_{(CCN)}22+\delta_{(CNC)}12$	570	559	$\gamma_{(CCCC)}13+\gamma_{(CPdCN)}18$
906	888	$\tau_{(HCCC)}91$	689	675	$\nu_{(PdN)}12$	1053	1020	$\nu_{(NC)}28+ \delta_{(CCN)}21+\delta_{(CNC)}11$	535	524	$\nu_{(CC)}14+\delta_{(CCN)}22+\delta_{(CNC)}12 +\delta_{(CCC)}14$
895	877	$\tau_{(HCCC)}50+$	670	657	$\tau_{(HNCN)}62$	1047	1012	$\tau_{(HCCC)}31+\gamma_{(CCCN)}13$	450	441	$\tau_{(CCCN)}23+ \gamma_{(CCCC)}36$
888	870	$\nu_{(ON)}46 +\tau_{(HCCC)}12+ \tau_{(HCCN)}23$	644	631	$\nu_{(NC)}13+\delta_{(CNC)}17+ \tau_{(HNCN)}10+\nu_{(BrC)}11$	1041	949	$\tau_{(HCCC)}52$	447	438	$\tau_{(CCCN)}24+ \gamma_{(CCCC)}45$
854	837	$\tau_{(HCCC)}74$	635	622	$\nu_{(NC)}19+\delta_{(CNC)}14+ \tau_{(HNCN)}16$	1033	926	$\tau_{(HCCN)}26+\tau_{(HCCC)}10$	433	424	$\delta_{(CCC)}75+\delta_{(PdNC)}10$
815	799	$\tau_{(HCCC)}10+ \tau_{(HCCN)}15+ \tau_{(CCCC)}10$	591	579	$\tau_{(HNCN)}67$	968	893	$\nu_{(CC)}25+\delta_{(CNC)}17$	430	421	$\delta_{(CCC)}61+\delta_{(CNPd)}10$
761	746	$\tau_{(CCCC)}12$	541	530	$\tau_{(CCCC)}15+\gamma_{(CPdCN)}15$	945	889	$\nu_{(CC)}17+\delta_{(CNC)}21$		287	$\nu_{(CC)}25+\delta_{(CNC)}17$
746	731	$\tau_{(CNCC)}65+ \tau_{(CCCC)}23$	530	519	$\tau_{(HCCC)}18+\tau_{(CCCC)}15$	911	881	$\tau_{(HCCC)}60$	338	285	$\nu_{(PdCl)}81$
706	692	$\nu_{(NC)}16+ \nu_{(ON)}21 +\delta_{(CCC)}12$	479	469	$\delta_{(CNC)}10+ \tau_{(CNCC)}12 +\gamma_{(CPdCN)}12$	907	744	$\tau_{(CCCN)}29+\gamma_{(PdCCN)}10$	335	257	$\nu_{(PdCl)}80$
680	666	$\delta_{(CCN)}66$	468	459	$\delta_{(CNC)}29+\tau_{(CNCC)}11$	899	732	$\delta_{(CCN)}20+\nu_{(NC)}11+ \nu_{(CC)}10$	302	253	$\delta_{(NPdN)}10 +\gamma_{(CCCC)}26$
655	642	$\delta_{(CCN)}73$	460	451	$\tau_{(HNCN)}35$	759	730	$\delta_{(CCN)}24+\nu_{(NC)}13+ \nu_{(CC)}11+\delta_{(CCN)}10$	298	3141	$\delta_{(CCC)}64+ \gamma_{(CCCC)}11$
598	586	$\gamma_{(OCON)}53$	447	438	$\tau_{(CNCC)}16+\tau_{(HNCN)}19$	747	558	$\nu_{(CC)}20+\nu_{(PdN)}15$ $\delta_{(CCC)}27$			
514	504	$\gamma_{(CCCC)}50$	444	435	$\tau_{(HNCN)}39+\gamma_{(CPdCN)}14$	745	556	$\nu_{(CC)}17+\nu_{(PdN)}15$ $\delta_{(CCC)}25$			

490	480	$\delta_{(ONO)}34+ \gamma_{(NCCC)}10+ \gamma_{(CCCC)}13+ \gamma_{(OCON)}27$	427	418	$\gamma_{(CPdCN)}60$	569	530	$\tau_{(CCCN)}13+\gamma_{(CCCC)}13$			
441	432	$\tau_{(HONC)}67$	337	286	$\nu_{(PdCl)}70$	567	527	$\nu_{(CC)}11+\delta_{(CCN)}10+ \gamma_{(CNCO)}11+\gamma_{(CPdCN)}12$			
424	416	$\tau_{(CCCC)}74+ \tau_{(HCCH)}12$	334	284	$\nu_{(PdCl)}73$	541	515	$\tau_{(CCCN)}84$			
411	403	$\tau_{(CCNPd)}53+ \tau_{(CNCC)}10+ \tau_{(HCCC)}14$	309	263	$\tau_{(CCCC)}13+\gamma_{(CPdCN)}16+ \gamma_{(BrCCC)}32$	538	490	$\gamma_{(CPdCN)}12$			
408	400	$\tau_{(CNCC)}55+ \tau_{(HCCC)}16$	302	257	$\tau_{(CCCC)}12+\gamma_{(CPdCN)}15+\gamma_{(BrCCC)}35+\nu_{(PdCl)}11$	525	426	$\delta_{(CCC)}20+ \gamma_{(CCNPd)}13+\tau_{(CCCN)}15$			
350	343	$\nu_{(PdCl)}22+ \delta_{(CCC)}12$	299	254	$\nu_{(PdCl)}13+ \nu_{(BrC)}39$	500	415	$\nu_{(PdCl)}95$			
339	332	$\nu_{(PdCl)}31$	294	250	$\nu_{(BrC)}52$	435	409	$\nu_{(PdCl)}91$			
312	306	$\nu_{(PdCl)}18$	262	223	$\nu_{(BrC)}10+\delta_{(BrCC)}35$	423	249	$\delta_{(NPdN)}21+\gamma_{(PdCCN)}11+ \gamma_{(CCCC)}10+\gamma_{(CNCC)}10$			
292	286	$\gamma_{(CCPdN)}12$	250	213	$\delta_{(BrCC)}48$	417	228	$\delta_{(ClPdN)}19$			
261	256	$\delta_{(CNPd)}11+ \gamma_{(NCCC)}11+ \gamma_{(CCPdN)}14$				293					

Table S2. Optimized parameters for the complexes (bond length and bond angles)

$PdCl_2L^4_2$				$[PdCl_2L^3_2]$				$[PdCl_2L^2_2]$				$[PdCl_2L^1_2]$			
Atoms	bond length (Å)	Atoms	bond angles (°)	Atoms	bond length (Å)	Atoms	bond angles (°)	Atoms	bond length (Å)	Atoms	bond angles (°)	Atoms	bond length (Å)	Atoms	bond angles (°)
Pd1-Cl2	2.27	Cl2-Pd1-Cl3	90.00	Pd1-Cl2	2.27	Cl2-Pd1-Cl3	90	Pd1-Cl2	2.27	Cl2-Pd1-Cl3	90	Pd1-Cl2	2.27	Cl2-Pd1-Cl3	90.00
Pd1-Cl3	2.27	Cl2-Pd1-N20	90.00	Pd1-Cl3	2.27	Cl2-Pd1-N20	90	Pd1-Cl3	2.27	Cl2-Pd1-N20	90	Pd1-Cl3	2.27	Cl2-Pd1-N22	90.00
Pd1-N20	2.05	Cl3.Pd1-N21	90.00	Pd1-N20	2.05	Cl3-Pd1-N21	90	Pd1-N20	2.05	Cl3-Pd1-N21	90	Pd1-N22	2.05	Cl3-Pd1-N23	90.00
Pd1-N21	2.05	N20-Pd1-N21	90.00	Pd1-N21	2.05	N20-Pd1-N21	90	Pd1-N21	2.05	N20-Pd1-N21	90	Pd1-N23	2.05	N22-Pd1-N23	90.00
C4-C6	1.40	C6-C4-H7	120.01	C4-C6	1.39	C6-C4-H7	120.01	C4-C6	1.39	C6-C4-H7	120.01	C4-C6	1.39	C6-C4-H7	120.01
C4-H7	1.10	C6-C4-N20	120.01	C4-H7	1.09	C6-C4-N20	120.00	C4-H7	1.09	C6-C4-N20	120.00	C4-H7	1.09	C6-C4-N22	120.01
C4-N20	1.39	H7-C4-N20	119.98	C4-N20	1.39	H7-C4-N20	119.98	C4-N20	1.39	H7-C4-N20	119.98	C4-N22	1.39	H7-C4-N22	119.98
C5-C8	1.39	C8-C5-H9	119.99	C5-C8	1.39	C8-C5-N20	120.0	C5-C8	1.39	C8-C5-N20	120.0	C5-C8	1.39	C8-C5-H9	119.99
C5-H9	1.10	C8-C5-N20	120.00	C5-C22	1.54	C8-C5-C22	119.9	C5-C22	1.47	C8-C5-C22	119.99	C5-H9	1.09	C8-C5-N22	120.00
C5-N20	1.39	H9-C5-N20	120.01	C5-N20	1.39	N20-C5-C22	120.00	C5-N20	1.39	N20-C5-C22	120.00	C5-N22	1.39	H9-C5-N22	120.01
C6-C10	1.39	C4-C6.C10	119.99	C6-C9	1.39	C4-C6-C9	119.99	C6-C9	1.39	C4-C6-C9	119.99	C6-C10	1.39	C4-C6-C10	119.99
C6-H11	1.09	C4-C6-H11	120.01	C6-H10	1.09	C4-C6-H10	120.01	C6-Br28	1.91	C4-C6-Br28	120.01	C6-H11	1.09	C4-C6-H11	120.01
C8-C10	1.39	C10.C6-H11	119.99	C8-C9	1.39	C9-C6-H10	119.99	C8-C9	1.39	C9-C6-Br28	119.99	C8-C10	1.39	C10-C6-H11	119.99
C8-C22	1.54	C5-C8-C10	120.01	C8-H11	1.09	C5-C8-C9	120.00	C8-H10	1.09	C5-C8-C9	120.00	C8-H12	1.09	C5-C8-C10	120.00
C10-C26	1.54	C5-C8-C22	119.98	C9-C30	1.54	C5-C8-H11	119.98	C9-H11	1.09	C5-C8-H10	119.98	C10-C24	1.54	C5-C8-H12	119.98
C12-C14	1.39	C10-C8-C22	120.01	C12-C14	1.39	C9-C8-H11	120.01	C12-C14	1.39	C9-C8-H10	120.01	C13-C15	1.39	C10-C8-H12	120.01
C12-H15	1.09	C6-C10-C8	119.99	C12-N21	1.39	C6-C9-C8	119.99	C12-N21	1.39	C6-C9-C8	119.99	C13-H16	1.09	C6-C10-C8	119.99
C12-N21	1.39	C6-C10-C26	119.98	C12-C26	1.54	C6-C9-C30	119.98	C12-N25	1.47	C6-C9-H11	119.98	C13-N23	1.39	C6-C10-C24	119.98
C13-C16	1.39	C8-C10-C26	120.03	C13-C15	1.39	C8-C9-C30	120.02	C13-C15	1.39	C8-C9-H11	120.02	C14-C17	1.39	C8-C10-C24	120.02
C13-H17	1.09	C14-C12-H15	120.01	C13-H16	1.09	C14-C12-N21	120.00	C13-H16	1.09	C14-C12-N21	120.00	C14-H18	1.09	C15-C13-H16	120.01
C13-N21	1.39	C14-C12-N21	120.00	C13-N21	1.39	C14-C12-C26	120.01	C13-N21	1.39	C14-C12-N25	120.01	C14-N23	1.39	C15-C13-N23	120.01
C14-C18	1.39	H15-C12-N21	119.98	C14-C17	1.39	N21-C12-C26	119.98	C14-C17	1.39	N21-C12-N25	119.98	C15-C19	1.39	H16-C13-N23	119.98
C14-C30	1.54	C16-C13-H17	119.99	C14-H18	1.09	C15-C13-H16	119.99	C14-H18	1.09	C15-C13-H16	119.99	C15-H20	1.09	C17-C14-H18	119.99
C16-C18	1.39	C16-C13-N21	120.00	C15-C17	1.39	C15-C13-N21	120.00	C15-C17	1.39	C15-C13-N21	120.00	C17-C19	1.39	C17-C14-N23	120.00
C16-H19	1.09	H17-C13-N21	120.00	C15-H19	1.09	H16-C13-N21	120.00	C15-Br29	1.91	H16-C13-N21	120.00	C17-H21	1.09	H18-C14-N23	120.01
C18-C34	1.54	C12-C14-C18	119.99	C17-C34	1.54	C12-C14-C17	119.99	C17-H19	1.09	C12-C14-C17	119.99	C19-C27	1.54	C13-C15-C19	119.99
C22-H23	1.07	C12-C14-C30	120.01	C22-H23	1.07	C12-C14-H18	120.01	N22-H23	1.00	C12-C14-H18	120.01	C24-H25	1.07	C13-C15-H20	120.01
C22-H24	1.07	C18-C14-C30	119.99	C22-H24	1.07	C17-C14-H18	119.99	N22-H24	1.00	C17-C14-H18	119.99	C24-H26	1.07	C19-C15-H20	119.99
C22-H25	1.07	C13-C16-C18	120.05	C22-H25	1.07	C13-C15-C17	120.00	N25-H26	1.00	C13-C15-C17	120.00	C24-C30	1.54	C14-C17-C19	120.00
C26-H27	1.07	C13-C16-H19	119.98	C26-H27	1.07	C13-C15-H19	119.98	N25-H27	1.00	C13-C15-Br29	119.98	C27-H28	1.07	C14-C17-H21	119.98
C26-H28	1.07	C18-C16-H19	120.01	C26-H28	1.07	C17-C15-H19	120.01			C17-C15-Br29	120.01	C27-H29	1.07	C19-C17-H21	120.01

C26-H29	1.07	C14-C18-C16	119.99	C26-H29	1.07	C14-C17-C15	119.99			C14-C17-C15	119.99	C27-C40	1.54	C15-C19-C17	119.99
C30-H31	1.07	C14-C18-C34	119.98	C30-H31	1.07	C14-C17-C34	119.98			C14-C17-H19	119.98	C30-C31	1.39	C15-C19-C27	119.98
C30-H32	1.07	C16-C18-C34	120.02	C30-H32	1.07	C15-C17-C34	120.02			C15-C17-H19	120.02	C30-C32	1.39	C17-C19-C27	120.02
C30-H33	1.07	Pd1-N20-C4	119.99	C30-H33	1.07	Pd1-N20—C4	119.99			Pd1-N20—C4	119.99	C31-C33	1.39	Pd1-N22-C4	120.00
C34-H35	1.07	Pd1-N20-C5	120.00	C34-H35	1.07	Pd1-N20-C5	120.00			Pd1-N20-C5	120.00	C31-H34	1.09	Pd1-N22-C5	120.00
C34-H36	1.07	C4-N20-C5	119.99	C34-H36	1.07	C4-N20-C5	119.99			C4-N20-C5	119.99	C32-C35	1.39	C4-N22-C5	120.00
C34-H37	1.07	Pd1-N21-C12	119.99	C34-H37	1.07	Pd1-N21-C12	119.99			Pd1-N21-C12	119.99	C32-H36	1.09	Pd1-N23-C13	120.00
		Pd1-N21-C13	120.00			Pd1-N21-C13	120.00			Pd1-N21-C13	120.00	C33-C37	1.39	Pd1-N23-C14	120.00
		C12-N21-C13	119.99			C12-N21-C13	119.99			C12-N21-C13	119.99	C33-H38	1.09	C13-N23-C14	120.00
		C8-C22-H23	109.47			C5-C22-H23	109.47			C5-C22-H23	109.47	C35-C37	1.39	C10-C24-H25	109.47
		C8-C22-H24	109.47			C5-C22-H24	109.47			C5-C22-H24	109.47	C35-H39	1.09	C10-C24-H26	109.47
		C8-C22-H25	109.47			C5-C22-H25	109.47			H23-C22-H24	109.47	C37-N50	1.47	C10-C24-C30	109.47
		H23-C22-H24	109.47			H23-C22-H24	109.47			C12-N25-H26	109.47	C40-C41	1.39		
		H23-C22-H25	109.47			H23-C22-H25	109.47			C12-N25-H27	109.47	C40-C42	1.39	H25-C24-H26	109.47
		H24-C22-H25	109.47			H24-C22-H25	109.47			H26-N25-H27	109.47	C41-C43	1.39	H25-C24-C30	109.47
		C10-C26-H27	109.47			C12-C26-H27	109.47					C41-H44	1.09	H26-C24-C30	109.47
		C10-C26-H28	109.47			C12-C26-H28	109.47					C42-C45	1.39	C19-C27-H28	109.47
		C10-C26-H29	109.47			C12-C26-H29	109.47					C42-H46	1.09	C19-C27-H29	109.47
		H27-C26-H28	109.47			H27-C26-H28	109.47					C43-C47	1.39	C19-C27-C40	109.47
		H27-C26-H29	109.47			H27-C26-H29	109.47					C43-H48	1.09	H28-C27-H29	109.47
		H28-C26-H29	109.47			H28-C26-H29	109.47					C45-C47	1.39	H28-C27-C40	109.47
		C14-C30-H31	109.47			C9-C30-H31	109.47					C45-H49	1.09	H29-C27-C40	109.47
		C14-C30-H32	109.47			C9-C30-H32	109.47					C47-N51	1.47	C24-C30-C31	120.00
		C14-C30-H33	109.47			C9-C30-H33	109.47					N50-O52	1.36	C24-C30-C32	120.00
		H31-C30-H32	109.47			H31-C30-H32	109.47					N50-O54	1.36	C31-C30-C32	120.00
		H31-C30-H33	109.47			H31-C30-H33	109.47					N51-O56	1.36	C30-C31-C33	120.01
		H32-C30-H33	109.47			H32-C30-H33	109.47					N51-O58	1.36	C30-C31-H34	119.98
		C18-C34-H35	109.47			C17-C34-H35	109.47					O52-H53	0.96	C33-C31-H34	120.01
		C18-C34-H36	109.47			C17-C34-H36	109.47					O54-55H	0.96	C30-C32-C35	120.00
		C18-C34-H37	109.47			C17-C34-H37	109.47					O56-H57	0.96	C30-C32-H36	120.01
		H35-C34-H36	109.47			H35-C34-H36	109.47					O58-H59	0.96	C35-C32-H36	119.99
		H35-C34-H37	109.47			H35-C34-H37	109.47							C31-C33-C37	119.99
		H36-C34-H37	109.47			C36-C34-H37	109.47							C31-C33-H38	120.01
														C37-C33-H38	119.99
														C32-C35-C37	120.00
														C32-C35-H39	119.98
														C37-C35-H39	120.01
														C33-C37-C35	119.99
														C33-C37.C35	119.99
														C33-C37-N50	119.98
														C35-C37-N50	120.02
														C27-C40-C41	120.00
														C27-C40-C42	120.00
														C41-C40-C42	120.00
														C40-C41-C43	120.01

														C40-C41-H44	119.98
														C43-C41-H44	120.01
														C40-C42-C45	120.00
														C40-C42-H46	120.01
														45-C42-H46	119.99
														C41-C43-C47	119.99
														C41-C43-H48	120.01
														C47-C43-H48	119.99
														C42-C45-C47	120.00
														C42-C45-H49	119.98
														C47.C45-H49	120.01
														C43-C47-C45	119.99
														C43-C47-N51	119.98
														C45-C47-N51	120.02
														C37-N50-O52	109.47
														C37-N50-O54	109.47
														O52-N50-O54	109.47
														C47-N51-O56	109.47
														C47-N51-O58	109.47
														O56-N51-O58	109.47
														N50-O52-H53	109.50
														N50-O54-H55	109.50
														N51-O56-H57	109.50

Table S3. Theoretical ^{1}H NMR and ^{13}C-NMR results for the complexes

$[PdCl_2L^1{}_2]$				$[PdCl_2L^2{}_2]$				$[PdCl_2L^3{}_2]$				$PdCl_2L^4{}_2$			
ATOM	Theoretical (ppm)	ATOM	Theoretical (ppm)	ATOM	Theoretical (ppm)	ATOM	Theoretical (ppm)	ATOM	Theoretical (ppm)	ATOM	Theoretical (ppm)	ATOM	Theoretical (ppm)	ATOM	Theoretical (ppm)
10,19 C	163,00	18 H	9,48	5 C	162,00	16H	8,57	5 C	174,51	7H	9,76	5 C	159,98	17H	9,24
5C	160,64	9 H	9,28	12 C	161,88	7H	8,46	12 C	172,89	11H	9,62	13 C	157,67	9H	9,14
14 C	160,46	7 H	8,34	13 C	154,65	19,11H	7,96	13 C	162,97	19,18H	8,21	12,10,18C	157,19	7H	8,12
13 C	157,79	49,16,38, 21,39,48H	8,11	4 C	154,49	18,1H	7,07	4 C	162,41	10H	8,11	4 C	154,79	15H	8,00
4C	157,63	11,34,46H	7,84	9 C	145,26	23,2H	6,91	17 C	155,26	23H	7,99	14 C	142,01	19H	7,92
47 C	156,90	12 H	7,62	17 C	145,11	26,2H	4,98	9 C	154,85	28H	5,96	8 C	141,78	11H	7,71
37 C	156,75	44,36 H	7,56	15 C	136,43			8 C	132,47	27H	4,60	6 C	131,19	28,27,35,36, 25,24H	2,48
30 C	142,43	20 H	7,47	6 C	136,26			14 C	131,65	24H	3,36	16 C	130,85	32,23,37,29, 31H	2,27
40 C	142,29	53,59 H	6,91	8 C	115,98			15 C	129,48	29H	2,76	34,26 C	27,16	33H	1,91
42,31C	136,69	57,55 H	6,82	14 C	115,81			6 C	128,88	35,32H	2,44	22 C	25,41		
41 C	136,32	29 H	4,31	5 C	162,00			26 C	42,51	25H	1,90	30 C	25,33		
32 C	136,18	26 H	4,21	12 C	161,88			22 C	38,76	31H	1,83				
6 C	132,56	28,25 H	4,07	13 C	154,65			34 C	26,86	36H	1,72				
15 C	132,45			4 C	154,49			30 C	26,77	37H	1,64				
8 C	132,16			9 C	145,26					33H	1,37				
17 C	131,95														
35 C	124,97														
43 C	124,88														
33 C	123,63														
45 C	123,20														
24 C	50,06														
27 C	50,01														